Optical properties of Sb-terminated GaAs and InP (110) surfaces

Paulo V. Santos, N. Esser, and M. Cardona
Max-Planck-Institut für Festkörperforschung, Heisenbergstrasse 1, D-70569 Stuttgart, Federal Republic of Germany

W. G. Schmidt and F. Bechstedt
Institut für Festkörpertheorie und Theoretische Optik, Friedrich-Schiller-Universität, Max-Wien-Platz 1, D-07743 Jena, Federal Republic of Germany

(Received 11 May 1995)

The dielectric function and the Raman scattering cross section for surface vibrations on InP and GaAs (110) surfaces terminated with an antimony monolayer were calculated using the empirical tight-binding method. The calculations reproduce well the surface dielectric function and its anisotropy. The Raman cross section for surface vibrations was determined for deformation-potential-induced scattering by calculating the changes in the dielectric function caused by the surface phonon eigenmodes. In agreement with the experimental results, the different surface phonon modes exhibit different resonance profiles since the coupling to the surface electronic states strongly depends on the respective atomic displacements. The results demonstrate that, as for the bulk case, resonant Raman scattering can be used to probe the surface electronic properties.

I. INTRODUCTION

Antimony forms a well-ordered epitaxial (1×1) monolayer on the (110) surfaces of a number of III-V compounds such as GaAs, InP, and InAs.[1–4] The interfaces between the Sb monolayer and the (110) substrate are abrupt and the Sb-terminated III-V surfaces, hereafter denoted as III-V (110):Sb, represent an ideal system for the investigation of the electronic structure of monolayer adsorbates. The most accepted model for the structure of the III-V (110):Sb surfaces is the epitaxial continued layer structure model.[1,3] According to this model, the surface Sb monolayer grows pseudomorphically on the (110) substrate forming chains along the $[1\bar{1}0]$ direction. The relaxation of the Sb and substrate atoms leads to a small displacement with respect to the crystalline positions, as illustrated in Figs. 1(a) and 1(b).

III-V (110):Sb surfaces have been intensively investigated by electron spectroscopy[3–7] and by tunneling microscopy.[8,9] More recently, experimental and theoretical techniques have been developed to probe the optical properties of III-V (110):Sb surfaces in the visible and ultraviolet energy range.[10–13] Most of the experimental investigations have been based on reflection difference and reflection anisotropy spectroscopy of Sb-covered GaAs and InP (110) surfaces. The Sb monolayer introduces surface states and resonances near the band edges of the (110) III-V semiconductor surfaces: an extensive description of the surface band structure is found in Refs. 14 and 15. The near gap states are very similar for all III-V substrates and arise from the bond between the Sb chains and the first substrate layer.[11,12,15]

The vibration of surface Sb atoms has been the subject of several theoretical[16–18] and experimental investigations[19–21]. Hünermann *et al.*[19] have demonstrated that the surface vibrational modes can be detected by Raman spectroscopy. Since the scattering intensity depends on the excited electronic states,[21] the investigation of the resonance Raman profile of the different vibrational modes provides a powerful probe of the surface electronic structure. Until now, the technique of resonant Raman scattering has only been applied to some of the surface vibrational modes of InP (110):Sb and

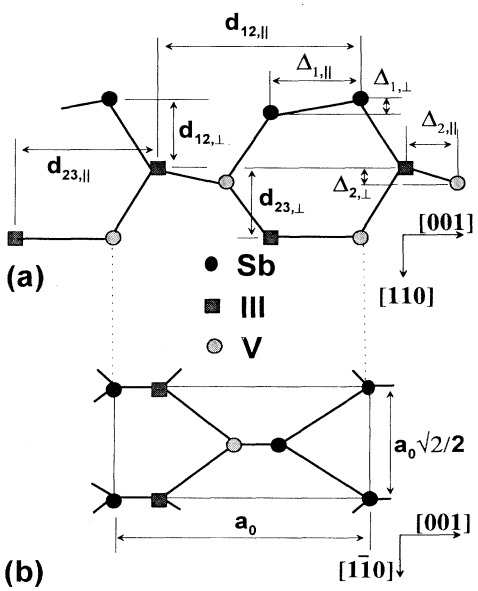

FIG. 1. Atomic structure of Sb-covered (110) III-V surface viewed along the (a) $[0\bar{1}1]$ and (b) [011] directions. In the convention used here, the x, y, and z axis are parallel to the $[1\bar{1}0]$, [001], and [110] directions, respectively.

 ©1995 The American Physical Society

GaAs (110):Sb. A theoretical understanding of the coupling between the surface vibrations and the electronic states is still lacking.

In this paper we use the empirical tight-binding method (ETBM) to calculate the dielectric function and the energy-dependent Raman cross section of GaAs (110):Sb and InP (110):Sb surfaces. Due to its computational simplicity, the ETBM can handle structures with a large number of atoms per unit cell, such as those necessary for the determination of the surface band structure and optical properties. The dielectric function and its orientation anisotropy are compared to experimental results. The Raman cross section was determined for deformation-potential-induced scattering by calculating the changes in the dielectric function caused by the surface phonon eigenmodes. In agreement with the experimental results, the different surface phonon modes exhibit different resonance profiles since the coupling to the surface electronic states strongly depends on the respective atomic displacements. The tight-binding calculations reproduce well the measured Raman cross section. The calculated Raman resonance profile and its polarization dependence can be understood using a bond polarizability model for the Raman cross section.

II. CALCULATION METHOD

A. Dielectric function

The structural model used in the ETBM calculations consists of a slab of 15–30 III-V atomic planes oriented perpendicularly to the [110] direction and terminated on both surfaces by Sb monolayers. As mentioned before (see also Fig. 1) the atomic positions near the surface differ from the bulk due to relaxation effects. In the ETBM calculations, we have used the atomic positions determined by means of total energy minimization using the first-principles pseudopotential method described in detail elsewhere.[17,22] The atomic positions, which are reproduced in Table I, are in good agreement with low-energy electron diffraction results.[23,24] For the clean surfaces, we used the atomic positions from Ref. 25. The same first-principles pseudopotential method was used to determine the vibrational properties of the antimony covered surfaces. The eigenvalues and eigenvectors were obtained by diagonalizing the dynamical matrix $\mathbf{K}$ and are listed for different surface modes in Table III. (See the discussion in Sec. II A.) The matrix elements $k^{ij}_{\alpha\beta}$ were obtained by displacing atom i from its equilibrium position in the direction α and calculating the forces acting on atom j in the direction β. Here $\alpha,\beta = (x,y,z)$ and $i,j = 1,N$, where N is the number of atoms in the three uppermost layers.

The ETBM calculation used a basis consisting of five sp^3s^* orbitals per atom[26] and did not include spin-orbit coupling. The slab calculations require the knowledge of the tight-binding matrix elements between anion and cation, anion and Sb, and Sb and cation. The parameters for GaAs and InP were obtained by a fit to the experimental energies at high-symmetry points of the band structure near the band gap.[26] The parameters describing the interaction between the Sb atoms and between the Sb and substrate atoms were obtained from those in GaSb (for GaAs substrates) and InSb for (InP substrates) following the procedure described in Ref. 15. The tight-binding parameters are summarized in Table II. The intersite parameters shown in the table were scaled using a $1/d^2$ law[27] so as to correspond to an effective crystal with the same bond length as the substrate. For this reason the Sb-Sb parameters for GaAs:Sb are different than those for InP:Sb.

The imaginary part of the dielectric function was calculated by integrating the matrix elements for optical transitions between the valence and conduction bands over the superlattice Brillouin zone of the repeated slab system. The optical transition elements were obtained directly from the tight-binding Hamiltonian using the procedure described in Refs. 28 and 29. In this way, no additional parameter other than those used to obtain the band structure is needed to determine the optical properties. The integration was performed by randomly sampling over many $\mathbf{k}$ points in the Brillouin zone (typically 750 $\mathbf{k}$ points for a slab of 30 atomic planes, corresponding to a unit cell containing 60 atoms).

It is convenient to express the optical properties of the surface layer in terms of the surface excess function (SEF).[30] The SEF has units of length and corresponds to the product of the dielectric function of the surface

TABLE I. Structural parameters for the clean (from Ref. 25) and for the Sb-covered (from Ref. 17) for GaAs (110) and InP (110) surfaces. The different displacements in units of Å are defined in Fig. 1. The $\perp$ and $\parallel$ subscripts denote displacements along the [110] and the [001] directions, respectively.

Surface	Clean GaAs (110)	GaAs (110):Sb	Clean InP (110)	InP (110):Sb
a_0	5.654	5.654	5.869	5.869
$\Delta_{1,\perp}$	0.684	0.05	0.753	0.16
$\Delta_{1,\parallel}$	1.205	2.0	1.215	1.98
$d_{12,\perp}$	2.036	2.37	2.048	2.44
$d_{12,\parallel}$	4.38	4.52	4.502	4.44
$\Delta_{2,\perp}$	0.0	0.09	0.0	0.07
$\Delta_{2,\parallel}$	1.414	1.41	1.467	1.46
$d_{23,\perp}$	1.999	2.01	2.075	2.04
$d_{23,\perp}$	2.827	2.73	2.934	2.77

TABLE II. Tight-binding parameters (in eV) used in the surface dielectric function calculations of GaAs (110):Sb and InP (110):Sb. The parameters for GaAs and InP stem from Ref. 26. The parameters describing the interaction between the Sb and substrates atoms were obtained from those in GaSb (for GaAs substrates) and InSb for (InP substrates) following the procedure described in Ref. 15. In this case, the intersite parameters shown in the table were scaled using a $1/d^2$ law[27] so as to correspond to an effective crystal with the same bond length as the substrate (for this reason the Sb-Sb parameters for GaAs are different than those for InP). The notation used corresponds to that of Ref. 29.

Atom 1-2	As-Ga	Sb-Ga	Sb-Sb (GaAs)	As-Sb	P-In	Sb-In	Sb-Sb (InP)	P-Sb
E_{s_1}	-8.343	-7.321	-7.321	-8.343	-8.527	-8.016	-8.016	-8.527
E_{p_1}	1.041	0.855	0.855	1.041	0.873	0.674	0.674	0.873
E_{s_2}	-2.657	-3.899	-7.321	-7.321	-1.483	-3.464	-8.016	-8.016
E_{p_2}	3.669	2.915	0.855	0.855	4.047	2.916	0.674	0.674
V_{ss}	-6.452	-7.208	-7.212	-7.212	-5.775	-7.246	-7.272	-7.273
V_{xx}	1.955	1.850	1.851	1.850	2.026	1.840	1.847	1.846
V_{xy}	5.079	4.833	4.835	4.837	4.560	5.090	5.107	5.108
V_{s_1p}	4.480	5.808	5.639	5.813	2.399	4.972	5.516	4.990
V_{s_2p}	5.783	5.465	5.639	5.469	6.014	6.024	5.516	6.045
$E_{s_1^*}$	8.591	6.635	6.635	8.591	8.264	6.454	6.454	8.264
$V_{s_1^*}$	4.843	5.843	5.395	5.848	3.730	4.681	4.592	4.697
$E_{s_2^*}$	6.739	5.985	6.635	6.635	7.067	5.936	6.454	6.454
$V_{s_2^*}$	4.808	4.938	5.395	4.941	4.830	4.469	4.592	4.484

layer (including the modification of the substrate dielectric properties near the surface) by its effective thickness. In the slab calculations, the SEF is obtained from the dielectric function of the clean ($\varepsilon_{\text{III-V}}$) and of the Sb-covered substrate ($\varepsilon_{\text{Sb:III-V}}$) through the expression

$$\text{SEF} = \tfrac{1}{2}(\varepsilon_{\text{Sb:III-V}} - \varepsilon_{\text{III-V}})d_{\text{slab}} \tag{1}$$

where d_{slab} is the slab thickness and the factor 1/2 accounts for the existence of two surfaces for each slab.

B. Raman cross section of surface phonons

Calculations of the Raman cross section of the surface phonons associated with the Sb monolayer require the knowledge of their vibrational eigenmodes. In the simplest approximation, these eigenmodes (and corresponding eigenfrequencies) are obtained by assuming the substrate atoms to be frozen. Since there are two Sb atoms per surface unit cell, there are four vibration eigenmodes corresponding to the six degrees of freedom of the Sb atoms minus the two translational modes parallel to the surface. This approximation was used by Godin *et al.*[18] to calculate the vibrational frequencies and displacements, as displayed in Fig. 2 (left panel) for GaAs (110):Sb. Despite its simplicity, this model reproduces well the observed vibrational frequencies.

The surface unit cell has a mirror plane parallel to the [001] direction (point group C_s). The vibration modes in Fig. 2 are denoted according to the symmetry with respect to the mirror plane (A' and A''). Modes with A' symmetry do not break the mirror symmetry and are thus expected to have diagonal Raman tensors,[19] i.e.,

$$R(A') = \begin{pmatrix} a & 0 \\ 0 & b \end{pmatrix}, \tag{2}$$

with respect to the principal optical axes $[0\bar{1}1]$ and [100]. Modes with A'' symmetry destroy the mirror plane and have an off-diagonal Raman tensor:

$$R(A'') = \begin{pmatrix} 0 & c \\ c & 0 \end{pmatrix}. \tag{3}$$

The observed selection rules for Raman scattering is in agreement with Eqs. (2) and (3).[19]

Due to the large mass of the Sb atoms, the mode frequencies in Fig. 2 lay within the vibrational continuum of the substrate and strongly mix with the III-V bulk-like vibrations. This effect was investigated recently by Schmidt and Srivastava,[16,17] who calculated the surface eigenmodes allowing the topmost (one to three) substrate atomic layers to vibrate. The number of eigenmodes increase with the number of vibrating atoms. We will concentrate throughout this paper only on the three lowest frequency A' modes ($1A'$ to $3A'$) and the A'' mode confined to the Sb and first substrate monolayers, which represent the surface phonons with strongest Raman cross section.[21] The eigenvectors for these modes, such as determined by the first-principles pseudopotential method described in Sec. II A, are listed in Table III and compared to those of Godin *et al.*[18] in Fig. 2 (right panel). Although the vibrational frequencies are not substantially affected for most of the A' modes, the vibrational eigenmodes are considerably different in the two cases. The A'' mode, on the other hand, remains unchanged and strongly confined to the Sb monolayer.

In this work the Raman scattering efficiency from surface phonons was calculated in the frozen phonon ap-

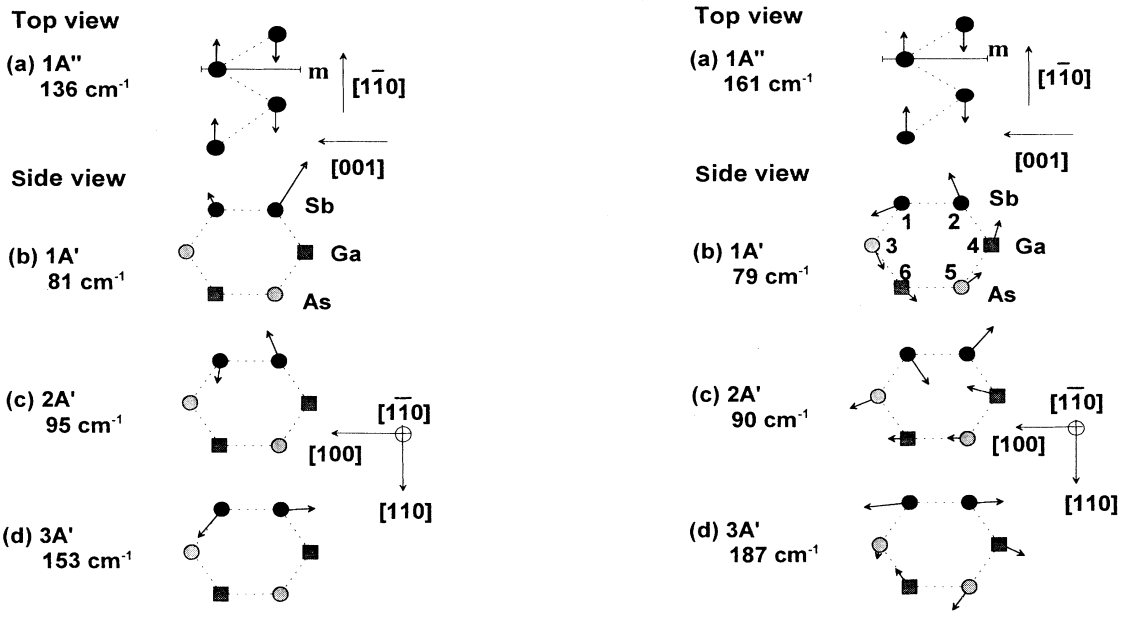

FIG. 2. Displacement eigenmodes for surface phonons in GaAs (110):Sb surfaces determined assuming that only the Sb atoms vibrate (left panel, from Ref. 18) and that the topmost three atomic layers vibrate (right panel). The vibration eigenmodes for the latter case were determined using the first-principles pseudopotential calculations described in Sec. II A and are also listed in Table III. [The atoms 1–6 are labeled according to (b) in the right panel.] The A'' mode is confined to the Sb top atoms and exhibits the same displacement pattern in both cases. This mode breaks the mirror symmetry plane of the surface unit cell, indicated by m in (a). The eigenmode for the A' modes, on the other hand, are considerably different in the two cases. The corresponding eigenmode frequencies are also indicated in the figure.

proach using the eigenmodes listed in Table III and displayed on the right side of Fig. 2. In this approach, the Stokes scattering efficiency S (in units of [length]$^{-1}$[solid angle(sr)]$^{-1}$) is related to the change in the dielectric function $\Delta\varepsilon$ induced by a phonon eigenmode of amplitude $\Delta\xi$ by[31]

$$S = \frac{\omega_s^4}{(4\pi c^2)^2}\frac{\hbar}{2\omega_p}V_c(n_{\mathrm{BE}}+1)\left|\left\langle \hat{\mathbf{e}}_\mathbf{s}\left|\frac{\Delta\varepsilon}{\Delta\xi}\right|\hat{\mathbf{e}}_\mathbf{i}\right\rangle\right|^2, \quad (4)$$

where ω_s (ω_p) is the light (phonon) frequency, n_{BE} is the Bose-Einstein factor, V_c is the unit cell volume, and $\hat{\mathbf{e}}_\mathbf{i}$ and $\hat{\mathbf{e}}_\mathbf{s}$ are the polarizations of the incident and scattered light.

In order to determine the derivative $\partial\varepsilon/\partial\xi$, the dielectric function was calculated for three values of the mode amplitude ξ. These three values were then fitted to a parabola in order to extract the linear term $\partial\varepsilon/\partial\xi$. The amplitudes ξ were chosen to be sufficiently small so as to yield maximum atomic displacements smaller than 2% of the bond length.

Equation (4) is well suited to describe the Raman efficiency of bulk materials. For the surface modes it is more convenient to express the Raman efficiency in terms of the total scattering efficiency (i.e., ratio between the scattering intensity per unit of solid angle and the incident light intensity), I_R. In the slab calculations, the latter is simply given by $I_R = (1/2)d_{\mathrm{slab}}S$, where the factor 1/2 again takes into account the existence of two Sb-covered surfaces for each slab.

III. RESULTS AND DISCUSSIONS

In Sec. III A we compare the tight-binding prediction for the surface dielectric function and dielectric anisotropy with experimental results. The tight-binding method reproduces relatively well the experiments, thereby justifying its use in Sec. III B for the determination of the energy-dependent Raman cross section of surface vibrations of InP:Sb and GaAs:Sb surfaces. The calculated cross sections are compared to experimental values and analyzed in terms of a bond polarizability model.

A. Dielectric function and anisotropy

The lines in Fig. 3 display the calculated imaginary part (ε_2) of the dielectric function of the clean (thin lines) and for a Sb-covered (thick lines) InP surface. The symbols show for comparison the same quantity measured at room temperature on a UHV cleaved (110) InP substrate.[32] The experimental spectrum is dominated by peaks at 3.15 and 4.7 eV associated with the bulk E_1 (and the spin-split component $E_1+\Delta_1 = 3.3$ eV) and E_0' transitions, respectively.[33] These transitions are reproduced in the calculated spectra, which, however, underestimate the amplitude of the high-energy structures. Also, the calculated E_1 transition is redshifted by 0.25 eV with respect to the experimental values. These discrepancies

TABLE III. Eigenfrequencies and eigenmodes of the first three atomic layers for surface modes of GaAs (110):Sb and InP (110):Sb surfaces. The atomic positions 1–6 are indicated in Fig. 1(b) (right panel). The x', y', and z' axes correspond to the [110], [0$\bar{1}$1], and [001] directions, respectively.

		GaAs (110):Sb				InP (110):Sb			
Mode	Atom	ω_p (cm^{-1})	x'	y'	z'	ω_p (cm^{-1})	x'	y'	z'
$1A'$	1	79	-0.425	0	-0.19	88.8	0.601	0	-0.258
	2		0.42	0	-0.173		-0.374	0	-0.258
	3		-0.324	0	0.163		0.136	0	0.189
	4		0.359	0	0.197		-0.159	0	0.484
	5		0.197	0	0.295		0.017	0	0.096
	6		-0.229	0	0.315		0.022	0	0.207
$2A'$	1	89.6	-0.43	0	0.268	143	0.294	0	-0.211
	2		0.414	0	0.312		0.328	0	0.199
	3		-0.108	0	-0.381		-0.113	0	0.084
	4		0.103	0	-0.395		-0.356	0	-0.171
	5		-0.015	0	-0.265		-0.182	0	-0.084
	6		0.07	0	-0.273		-0.217	0	-0.022
$3A'$	1	187	-0.084	0	-0.594	169	-0.248	0	-0.41
	2		0.027	0	0.488		0.43	0	0.179
	3		-0.048	0	-0.002		-0.046	0	0.008
	4		-0.145	0	0.375		-0.423	0	0.441
	5		0.316	0	-0.211		-0.006	0	-0.055
	6		0.248	0	-0.177		0.393	0	-0.141
A''	1	161	0	-0.705	0	158	0	-0.711	0
	2		0	0.708	0		0	0.703	0
	3		0	-0.021	0		0	-0.008	0
	4		0	0.009	0		0	0.003	0
	5		0	-0.004	0		0	-0.002	0
	6		0	0.012	0		0	0.009	0

are not only a limitation of the simple nearest-neighbor tight-binding model used here, which is only accurate for states close (i.e., a few eV away) from the band edges, but also consequences of the neglect of local field and excitonic effects.

The calculated spectra in Fig. 3 indicate that the main contributions of the Sb monolayer to the dielectric function occur for energies between 2 and 3 eV, i.e., below the bulk InP E_1 transition. This effect is further substantiated in Figs. 4 and 5, which compare the calculated SEF and reflection difference spectra (RDS) of clean and Sb-covered InP (110) surfaces with experimental values.[21] The RDS data correspond to the difference $(r_{[100]} - r_{[1\bar{1}0]})/\bar{r}$ between the complex reflection coefficient r for polarization along the surface principal optical axes [001] and [1$\bar{1}$0]. The calculations reproduce the main features of the measured spectra. The agreement

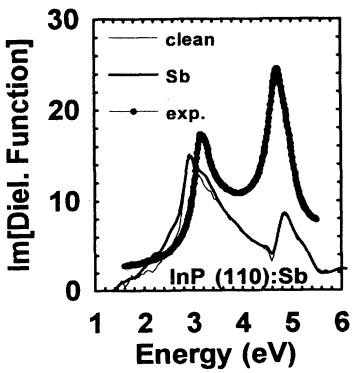

FIG. 3. Calculated imaginary part of the dielectric function for a clean (thin lines) and for a Sb-covered (thick line) InP (110) surface. The calculations were performed for a 60-Å InP (110) slab. For comparison, the symbols reproduce the imaginary part of the pseudodielectric function determined by spectroscopic ellipsometry on a cleaved InP (110) surface (Ref. 32).

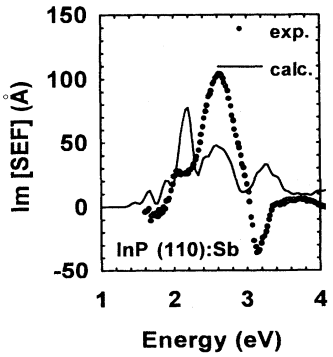

FIG. 4. Comparison between the experimental (symbols) and calculated (lines) surface excess function (SEF) for InP (110):Sb surfaces. The calculated data were determined from the difference between the dielectric functions of the Sb-covered and the clean InP (110) surfaces (see also Fig. 3). The experimental data were obtained from the changes induced by Sb adsorption in the pseudodielectric function measured by spectroscopic ellipsometry (Ref. 32).

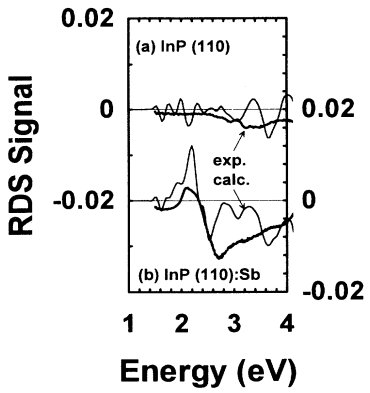

FIG. 5. Comparison between the real part of the experimental (symbols, from Ref. 21) and calculated (symbols) reflection difference spectra [RDS signal = $\mathrm{Re}(r_{[001]} - r_{[1\bar{1}0]})/\bar{r}$] for InP (110):Sb surfaces. The calculated data were determined from the difference between the dielectric functions evaluated for polarizations along the [100] and [1$\bar{1}$0] principal axes.

is better for the RDS results, indicating that some of the errors in the surface excess function calculation cancel out in the determination of the dielectric anisotropy. The surface excess function is dominated by maxima at 2.05 eV and at 2.65 eV, and by a minimum near the bulk E_1 transition at 3.15 eV (the corresponding structures in the calculated curves are found at 2.15, 2.65, and 3 eV, respectively). The RDS data indicate that the first transition is strongly polarized along the [001] direction (i.e., perpendicular to the Sb chains), whereas the second is stronger for the [1$\bar{1}$0] polarization. Similar results were also obtained for GaAs (110):Sb.

The assigment of the structures in Figs. 4 and 5 to transitions in the surface band structure is a difficult task since they involve excitations between unoccupied (valence) and occupied (conduction band) states whose energies depend on the **k** vector. We verified that it is not possible to account for the spectral shape in Figs. 4 and 5 by only taking into account transitions at the high-symmetry Brillouin zone points Γ, X, X'. Chiaradia *et al.*[11] and Esser *et. al.*[12] analyzed the experimental features by computing the contributions of transitions involving surface states to the RDS spectra of GaAs (110):Sb and InP (110):Sb surfaces. They attributed the structures in the RDS spectra for energies below 2.7 eV to transitions involving surfaces states (mainly the states S_6 to S_8 associated with bonding and antibonding states of the bonds between the Sb chain and the first substrate atomic layer[14,15]). The structures at higher energies are dominated by transitions involving bulk states modified by the presence of the surface.

B. Raman resonances

Before applying the tight-binding method to surface phonons, we used it to calculate the Raman efficiency S for bulk GaAs and bulk InP. The theoretical results are compared to experimental ones in Figs. 6(a) and 6(b). The absolute scattering intensity for GaAs was extracted from Refs. 34 and 35. The corresponding data for InP were obtained by combining the relative cross sections reported in Ref. 36 with absolute values determined near the E_0 gap by Kauschke and Cardona.[37] The Raman efficiency strongly resonates near the E_1 gap (2.95 and 3.15 eV in GaAs and InP, respectively). Except for the energy shifts mentioned previously, the resonance line shape is well reproduced by the calculated spectra (lines in Fig. 6). Note that the small shoulder in the GaAs curve at 2 eV is also present in the calculated data. As expected from the one-electron approximation, the tight-binding calculation cannot reproduce the excitonic enhancement of the Raman intensity near the E_0 gap.[38]

After this reliability test, the tight-binding method was used to calculate the resonance profile for the GaAs (110):Sb and InP (110):Sb surface phonons (Figs. 7 and 8, respectively). In the calculations we used the phonon eigenmodes listed in Table III, which were obtained under the assumption that the three topmost surface layers are free to vibrate (solid lines). The calculated Raman scattering intensity I_R represents the ratio between the scattering intensity per unit solid angle for the surface phonons and the incident laser intensity. The calculations were performed for the different modes displayed in Table III. For the A'' mode (upper left plots) the curves

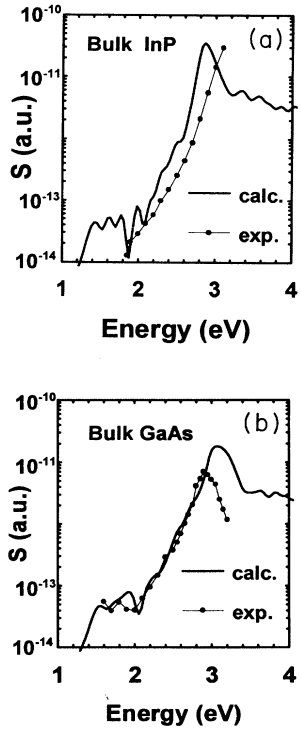

FIG. 6. Raman scattering efficiency, S [in atomic units, (bohr sr)$^{-1}$] for bulk TO phonons in (a) InP and (b) GaAs. The symbols reproduce the measured values for InP (Refs. 34 and 35) and GaAs (Refs. 37 and 36).

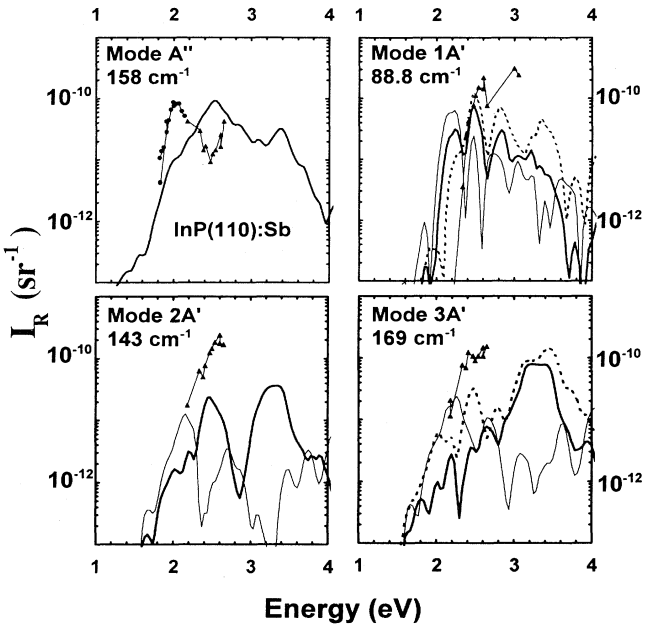

FIG. 7. Calculated Raman scattering intensity I_R (ratio between the scattering intensity per unit solid angle and the laser incident intensity), for InP (110):Sb surface phonons. For the diagonal modes $1A'$, $2A'$, and $3A'$, the thick (thin) lines correspond to the resonance behavior of the a (b) Raman tensor component [see Eq. (2)]. The calculations were performed for the different modes displayed in Table III, assuming that the three topmost surface layers vibrate. The dashed lines indicate the resonance profile for the $1A'$ and $3A'$ modes calculated using the eigenmode obtained when only the two topmost layers are allowed to vibrate. The solid triangles and circles display the measured Raman intensities reported in Refs. 21 and 32.

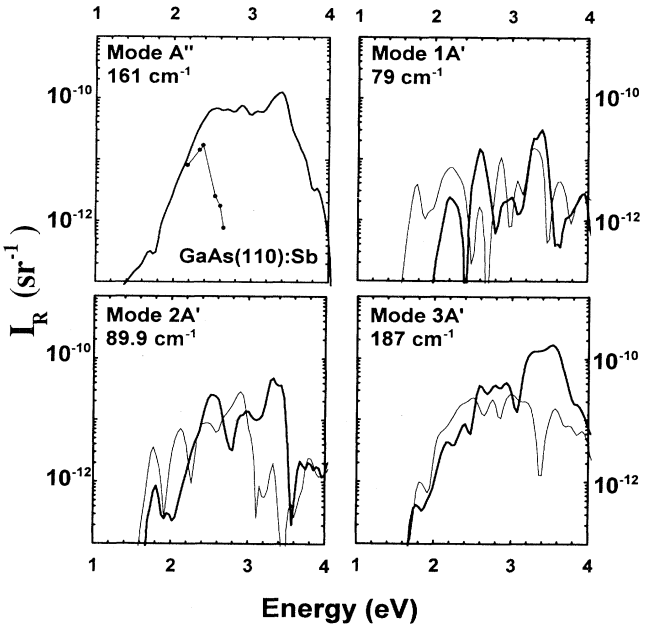

FIG. 8. Calculated Raman scattering intensity I_R (ratio between the scattering intensity per unit solid angle and the laser incident intensity), for surface phonons in GaAs (110):Sb surfaces. The calculations were performed for the different modes displayed in Fig. 2(b) and Table III, which were determined assuming that the three topmost surface layers are free to vibrate. For the diagonal modes $1A'$, $2A'$, and $3A'$ the thick (thin) lines correspond to the resonance behavior of the a (b) Raman tensor component [see Eq. (2)]. The solid triangles and circles display the measured Raman intensities reported in Ref. 21.

represent the resonance profile for the c component of the Raman tensor [see Eq. (3)]. For the diagonal modes (with respect to the principal axes $[1\bar{1}0]$ and [001]) $1A'$, $2A'$, and $3A'$ the thick (thin) lines correspond to the resonance behavior of the a (b) Raman tensor component [see Eq. (2)].

The triangles and circles display experimental data for the absolute Raman intensity obtained from Refs. 21 and 32, respectively. For the diagonal modes in InP (110):Sb, the experimental data were recorded with incoming and scattered radiation polarized along the $[1\bar{1}0]$ direction and correspond thus to the calculated curves displayed by the thick lines. There are presently no experimental data available for the other configuration, nor for the Raman resonance of the A' modes in GaAs.

The resonance behavior of the surface phonon modes differs considerably from that of the bulk materials (see Fig. 6) and exhibit maxima in the energy range from 2 to 3 eV, where the dielectric properties are dominated by transitions involving surface states. The A'' mode has a simple displacement pattern involving the vibration of only the top Sb atoms. In the calculations this mode resonates in InP (110):Sb at $\sim$ 2.7 eV, with a shoulder at 2 eV. These two energies correspond closely to the maxima in the SEF and RDS spectra. The experimental resonance data, on the other hand, shows a pronounced peak at 2 eV. These discrepancies, which are also observed for GaAs, are presently not understood. We note, however, the remarkable ability of the calculations to predict the order of magnitude and the line shape of the experimental scattering efficiencies. One can speculate that the overestimation of the Raman cross section in the high-energy range is related to an incorrect description of the optical matrix elements by the tight-binding parameters.[28,29].

The three A' modes exhibit different resonance profiles for the a and b components, with the first dominating at 2.7 eV and the second at 2.0 eV in both InP and GaAs. Note that this polarization dependence mimics that observed in the RDS spectra with stronger intensities for polarization along the $[1\bar{1}0]$ and [001] around 2.7 and 2 eV, respectively. The calculated profiles for the $1A'$ and $2A'$ mode reproduce relatively well the measured data in InP (110):Sb. The calculated intensities, however, underestimate the experimental values by a factor of 2–10. We recall here that the single-particle tight-binding method also underestimates the absolute cross sections of the InP bulk phonons [see Fig. 6(a)], since the Coulomb enhancement of the oscillator strengths is not taken into account.

For the $3A'$ mode, the difference between calculated and measured intensities are more pronounced than for the $1A'$ and $2A'$ modes. As indicated in Fig. 2 (right panel, see also Table III) the eigenmodes for the three A' modes penetrate considerably in the bulk and we trace this discrepancy to the errors introduced by neglecting the vibration of the deeper substrate layers. This effect is illustrated by the dashed lines for the $1A'$ and for the $3A'$ modes in Fig. 7, which display the resonance profile for the a-Raman tensor component under the assumption that only the two (instead of three for the thick solid line) topmost layers vibrate. The $1A'$ mode is not considerably affected but large differences are seen for the $3A'$ mode, whose eigenmode strongly depends on the number of vibrating atoms. This result illustrates the importance of using realistic phonon eigenmodes in the calculation of the Raman scattering intensities.

In the following, we present a simple argument based on the bond polarizability model to explain the line shape of resonance Raman profiles displayed in Figs. 7 and 8. We will focus the discussion on the GaAs (110):Sb system: Due to the similarity in the band structure, the same conclusions also hold for InP (110):Sb. In the bond polarizability model, the susceptibility is expressed as a sum of local contribution from single bonds. For each bond we associate energy-dependent polarizabilities $\alpha_{\parallel}$ and $\alpha_{\perp}$ for electric fields parallel and perpendicular to the bond axis, respectively. The dielectric function is obtained by adding the polarizability of the different bonds. The Raman scattering intensity can then be determined from the change in the total polarizability α_T induced by the phonon eigenmodes, i.e., $I_R \sim |\partial\alpha_T/\partial\xi|^2$. The phonon-induced modulation of the bond polarizability depends to first order on the modification of the bond angle and of the bond length R by the atomic displacements. The former is proportional to the difference $\Delta\alpha = \alpha_{\parallel} - \alpha_{\perp}$ between the polarizability perpendicular and parallel to the bond. The bond length contribution depends on the variation of $\alpha_{\parallel}$ and $\alpha_{\perp}$ with the bond length, described by the parameters $\Delta\alpha'_{\parallel} = \partial\alpha_{\parallel}/\partial \ln R$ and $\Delta\alpha'_{\perp} = \partial\alpha_{\perp}/\partial \ln R$, respectively.[31] In the following we will assume that $\Delta\alpha'_{\parallel} \gg \Delta\alpha'_{\perp}$, an approximation that holds for germanium, silicon, and diamond.[39] In this case, the following expression for the Raman tensor components of the GaAs surface modes is obtained from the eigenmodes of Table III:

$$\begin{aligned} c(1A'') \sim\ & +0.0016\Delta\alpha_{\text{Sb-Sb}} + 0.0160\Delta\alpha_{\text{As-Ga}} \\ & -0.0585\Delta\alpha_{\text{Sb-Ga}} - 0.0546\Delta\alpha_{\text{Sb-As}} \\ & +0.2085\Delta\alpha'_{\parallel,\text{Sb-Sb}} - 0.0096\Delta\alpha'_{\parallel,\text{As-Ga}} \\ & -0.0043\Delta\alpha'_{\parallel,\text{Sb-Ga}} - 0.0046\Delta\alpha'_{\parallel,\text{Sb-As}}\ , \end{aligned} \tag{5}$$

$$\begin{aligned} a(1A') \sim\ & -0.0098\Delta\alpha_{\text{Sb-Sb}} + 0.0123\Delta\alpha_{\text{As-Ga}} \\ & +0.0042\Delta\alpha'_{\parallel,\text{Sb-Sb}} - 0.0058\Delta\alpha'_{\parallel,\text{As-Ga}}, \end{aligned} \tag{6}$$

$$\begin{aligned} b(1A') \sim\ & -0.0012\Delta\alpha_{\text{Sb-Sb}} - 0.0245\Delta\alpha_{\text{As-Ga}} \\ & +0.0625\Delta\alpha_{\text{Sb-Ga}} - 0.0515\Delta\alpha_{\text{Sb-As}} \\ & +0.0055\Delta\alpha'_{\parallel,\text{Sb-Sb}} + 0.0077\Delta\alpha'_{\parallel,\text{As-Ga}} \\ & +0.0100\Delta\alpha'_{\parallel,\text{Sb-Ga}} - 0.0109\Delta\alpha'_{\parallel,\text{Sb-As}}\ , \end{aligned} \tag{7}$$

$$\begin{aligned} a(2A') \sim\ & -0.0159\Delta\alpha_{\text{Sb-Sb}} - 0.0244\Delta\alpha_{\text{As-Ga}} \\ & +0.0071\Delta\alpha'_{\parallel,\text{Sb-Sb}} + 0.0123\Delta\alpha'_{\parallel,\text{As-Ga}}, \end{aligned} \tag{8}$$

$$\begin{aligned} b(2A') \sim\ & +0.0061\Delta\alpha_{\text{Sb-Sb}} + 0.0000\Delta\alpha_{\text{As-Ga}} \\ & -0.1320\Delta\alpha_{\text{Sb-Ga}} + 0.1186\Delta\alpha_{\text{Sb-As}} \\ & +0.0105\Delta\alpha'_{\parallel,\text{Sb-Sb}} + 0.0037\Delta\alpha'_{\parallel,\text{As-Ga}} \\ & -0.0140\Delta\alpha'_{\parallel,\text{Sb-Ga}} + 0.0118\Delta\alpha'_{\parallel,\text{Sb-As}}\ , \end{aligned} \tag{9}$$

$$\begin{aligned} a(3A') \sim\ & -0.2772\Delta\alpha_{\text{Sb-Sb}} + 0.1766\Delta\alpha_{\text{As-Ga}} \\ & +0.1173\Delta\alpha'_{\parallel,\text{Sb-Sb}} - 0.0871\Delta\alpha'_{\parallel,\text{As-Ga}}, \end{aligned} \tag{10}$$

$$\begin{aligned} b(3A') \sim\ & +0.2758\Delta\alpha_{\text{Sb-Sb}} - 0.0543\Delta\alpha_{\text{As-Ga}} \\ & -0.0136\Delta\alpha_{\text{Sb-Ga}} - 0.0774\Delta\alpha_{\text{Sb-As}} \\ & +0.2033\Delta\alpha'_{\parallel,\text{Sb-Sb}} - 0.0446\Delta\alpha'_{\parallel,\text{As-Ga}} \\ & +0.0068\Delta\alpha'_{\parallel,\text{Sb-Ga}} - 0.0163\Delta\alpha'_{\parallel,\text{Sb-As}}\ . \end{aligned} \tag{11}$$

In each of these equations, the first and second lines correspond, respectively, to the first-order contributions of bond angle and bond length variations to the Raman components.

An interesting aspect of Eqs. (5)–(11) is the independence of the diagonal Raman tensor component a (modes $1A'$ to $3A'$) on the polarizabilities of the Sb-Ga and Sb-As bonds and their derivatives. This effect, which strictly holds only under the assumption of $\Delta\alpha'_{\perp} = 0$, can be understood by considering the displacement patterns of Fig. 2(b)–2(d) (left panel). The Sb-Ga and Sb-As bonds and the eigenmode for the diagonal modes lie in the $[1\bar{1}0]$ plane (the plane of the figure). As a result, the vibrations do not modulate the polarizability in the direction perpendicular to that plane (i.e., along the $[1\bar{1}0]$ direction), leading to a vanishing a component. This result will be important in understanding the resonance behavior of the Raman profile, as discussed in the following.

The bond polarizability model provides a local description of the optical properties and predicts maxima in the Raman intensity when the laser energy matches the transition energy between bonding and antibonding states of the bonds modified by the phonons. In a solid, however, there can be transitions involving states associated with different bonds. One then expects a resonance whenever at least one of the states involved in the transition is associated with a bond that has been modified by the phonon. As a result, the resonance behavior is considerably more complicated than that given in Eqs. (5)–(11), which implicitly assumes constant bond polarizabilities. Nevertheless, we show below that the bond polarizability model can qualitatively explain most of the features of the resonance profile.

The bonds between the Sb chain atoms and the first substrate layer (Sb-As and Sb-Ga bonds) are responsible for the states lying close to the bulk valence and conduction band edges (states S_5, S_4, S_7, and S_8, see Ref. 15). Transitions involving the corresponding bands lead to the SEF and RDS structures at ~ 2 eV. Accordingly, the Raman tensor components $c(1A'')$ and $b(1A') - b(3A')$, which are affected by these bonds [Eq. (11)], also resonate in the same energy range (see thin lines in Figs. 8 and 7). In the bond polarizability approximation described above, these bonds do not contribute to the a

Raman tensor components. As a result, the a component exhibits small values for energies below 2.7 eV (thick lines in Figs. 8 and 7).

The SEF and RDS resonances around 2.7 eV, on the order hand, are dominated by transitions involving states of the Sb-Sb (states S_3 and S_4) bonds and of the Ga-As bonds (states A_1' and A_2'). Since the S_3 and S_4 states lie at least 4 eV below the conduction band, the resonance of the a, b, and c Raman component is probably determined by the contributions from the states of Ga-As bond located near the surface. The bond polarizability model thus provides a qualitative explanation of the polarization dependence and of the resonance behavior of the Raman cross section.

IV. CONCLUSIONS

We have used the empirical tight-binding model to calculate the dielectric function and the Raman scattering cross sections for surface phonons of GaAs (110):Sb and InP (110):Sb surfaces. Despite its simplicity, the tight-binding method reproduces reasonably well the experimental results, including the absolute scattering intensities. The theoretical results are interpreted in terms of a simple bond polarizability model for the Raman cross section, which qualitatively describes the resonance behavior and the polarization dependence of the Raman cross section.

ACKNOWLEDGMENTS

We thank G.P. Srivastava for his collaboration in calculating the phonon modes and M. Chamberlain for discussions and for a critical reading of the manuscript. The authors are also indebted to H. Hirt, M. Siemers, and P. Wurster for technical assistance.

[1] P. Skeath, I. Lindau, C.Y. Su, and W.E. Spicer, J. Vac. Sci. Technol. **19**, 556 (1981).
[2] C. Mailhiot, C.B. Duke, and D.J. Chadi, Phys. Rev. Lett. **53**, 2114 (1984).
[3] C.B. Duke, A. Paton, W.K. Ford, A. Kahn, and J. Carelli, Phys. Rev. B **26**, 804 (1982).
[4] W.K. Ford, T. Guo, S.L. Lantz, K. Wan, S.-L. Chang, and C.B. Duke, J. Vac. Sci. Technol. B **8**, 940 (1990).
[5] P. Mårtensson, G.V. Hansson, M. Lähdeniemi, K.O. Margunsson, S. Wiklung, and J.M. Nichols, Phys. Rev. B **33**, 7399 (1986).
[6] A. Tulke and H. Lüth, Surf. Sci. **178**, 131 (1986).
[7] F. Schäffler, R. Ludeke, A. Taleb-Ibrahimi, G. Hughes, and D. Rieger, Phys. Rev. B **36**, 1328 (1987).
[8] R.M. Feenstra and P. Mårtensson, Phys. Rev. Lett. **61**, 447 (1988).
[9] P. Mårtensson and R.M. Feenstra, Phys. Rev. B **39**, 7744 (1989).
[10] M. Mattern-Klosson, R. Strämpler, and H. Lüth, Phys. Rev. B **33**, 2559 (1986).
[11] P. Chiaradia, A.I. Shkrebtii, C. Goletti, Wang Jian, and R. del Sole, Solid State Commun. **85**, 497 (1993); **89**, 87 (1994).
[12] N. Esser, M. Köpp, P. Haier, and W. Richter, J. Electron Spectrosc. **64&65**, 85 (1993).
[13] N. Esser, W. Richter, U. Resch-Esser, P. Chiaradia, C. Goletti, and L. Moretti, Philos. Mag. B **70**, 507 (1994).
[14] C.M. Bertoni, C. Calandra, F. Manghi, and E. Molinari, Phys. Rev. B **27**, 1251 (1983).
[15] C. Mailhiot, C.B. Duke, and D. J. Chadi, Phys. Rev. B **31**, 2213 (1985).
[16] W.G. Schmidt and G. P. Srivastava, Solid State Commun. **89**, 345 (1994).
[17] W.G. Schmidt and G. P. Srivastava, Surf. Sci. **331-333**, 540 (1995).
[18] T.J. Godin, J.P. LaFemina, and C.B. Duke, J. Vac. Sci. Technol. B **9**, 2281 (1991).
[19] M. Hünermann, J. Geurts, and W. Richter, Phys. Rev. Lett. **66**, 640 (1991).
[20] W. Richter, N. Esser, A. Kelnberger, and M. Köpp, Solid State Commun. **84**, 165 (1992).
[21] N. Esser, R. Hunger, J. Rumberg, W. Richter, R. del Sole, and A.I. Shkrebtii, Surf. Sci **307-309**, 1045 (1993).
[22] F. Bechstedt, W.G. Schmidt, and B. Wenzien, Europhys. Lett. **25**, 357 (1994); W.G. Schmidt, B. Wenzien, and F. Bechstedt, Phys. Rev. B **49**, 4731 (1994).
[23] W.K. Ford, T. Guo, D.L. Lessor, and C.B. Duke, Phys. Rev. B **42**, 8952 (1990).
[24] W.K. Ford, T. Guo, K.-J. Wan, and C.B. Duke, Phys. Rev. B **45**, 11 896 (1992).
[25] C. Mailhiot, C.B. Duke, and D. J. Chadi, Surf. Sci. **149**, 366 (1985).
[26] P. Vogl, H. Hjalmarson, and J. Dow, J. Phys. Chem. Solids **44**, 365 (1983).
[27] W.A. Harrison, *Electronic Structure and the Properties of Solids* (Dover Publications, New York, 1989), p. 48.
[28] G. Dresselhaus and M.S. Dresselhaus, Phys. Rev. **160**, 649 (1967).
[29] L.C. Lew Yan Voon and L.R. Ram-Mohan, Phys. Rev. B **47**, 15 500 (1993).
[30] M. Kelly, S. Zollner, and M. Cardona, Surf. Sci. **285**, 282 (1993).
[31] M. Cardona, in *Light Scattering in Solids II*, edited by M. Cardona and G. Güntherodt (Springer-Verlag, Berlin, 1982), p. 19.
[32] N. Esser and P.V. Santos (unpublished).
[33] *Semiconductors Physics of Group IV Elements and III-V Compounds*, edited by O. Madelung, Landolt-Börnstein, New Series, Group III, Vol. 17, Pt. a (Springer-Verlag, Heidelberg, 1982).
[34] M. Cardona, in *Light Scattering in Solids*, edited by J. L. Birman and H. Z. Cummins (Plenum Press, New York, 1979), p. 249.
[35] R. Trommer and M. Cardona, Phys. Rev. B **17**, 1865

(1978).
[36] M. Sinyukov, R. Trommer, and M. Cardona, Phys. Status Solidi B **86**, 563 (1978).
[37] W. Kauschke and M. Cardona, Phys. Rev. B **33**, 5473 (1986).
[38] A. Cantarero, C. Trallero-Giner, and M. Cardona, Phys. Rev. B **39**, 8388 (1989).
[39] Using the bond polarizability data listed on page 67 of Ref. 31 we calculated ratios $(\partial\alpha_\perp/\partial R)/(\partial\alpha_\parallel/\partial R) = 0.34$, 0.28, and 0 for bulk germanium, silicon, and diamond. The small values for this ratio justifies the approximations used in the bond polarizability model described in the text.